Crystal morphology and nucleation in thin films of amorphous Te alloys used for phase change recording

J. A. Kalb,[a] C. Y. Wen, and Frans Spaepen[b]
Division of Engineering and Applied Sciences, Harvard University, Cambridge, Massachusetts

H. Dieker and M. Wuttig
I. Physikalisches Institut der Rheinisch-Westfälische Technische Hochschule (RWTH) Aachen, 52056 Aachen, Germany

(Received 28 April 2005; accepted 20 July 2005; published online 6 September 2005)

Ex situ transmission electron microscopy (TEM) was used to study the crystal morphology in sputtered amorphous $Ge_4Sb_1Te_5$, $Ge_2Sb_2Te_5$, and $Ag_{0.055}In_{0.065}Sb_{0.59}Te_{0.29}$ thin films used for phase change recording. Tilting of plan view samples revealed that each crystallized growth formation is a bent single crystal. Cross-sectional TEM showed that crystals only nucleate heterogeneously at the (naturally oxidized) film surface. These findings allow the determination of nucleation parameters around 150 °C from earlier experiments [J. Kalb, F. Spaepen, and M. Wuttig, Appl. Phys. Lett. **84**, 5240 (2004)]. The time lag for nucleation has an activation energy of (2.74 ± 0.13) eV for $Ge_2Sb_2Te_5$ and (2.33 ± 0.18) eV for $Ag_{0.055}In_{0.065}Sb_{0.59}Te_{0.29}$. The activation energies for the steady-state nucleation rate were (4.09 ± 0.20) eV for $Ge_4Sb_1Te_5$ and (3.50 ± 0.17) eV for $Ge_2Sb_2Te_5$. With the activation energy for the crystal-growth velocity found in the earlier article the critical work for formation of the nucleus was found to be (1.35 ± 0.23) eV for $Ge_4Sb_1Te_5$ and (1.15 ± 0.22) eV for $Ge_2Sb_2Te_5$. These values are lower limits for homogeneous nucleation. © *2005 American Institute of Physics*. [DOI: 10.1063/1.2034655]

I. INTRODUCTION

Tellurium alloys are used for phase change recording in commercial rewritable storage devices. In rewritable (RW) compact disks (CDs) and digital video disks (DVDs), a thin film of a Te alloy is locally and reversibly switched by laser heating between the amorphous and the crystalline state. These states can be distinguished optically by their difference in reflectivity.[1] Recently, Te alloys have also shown high potential for future electronic nonvolatile data storage.[2] In these so-called *phase change random access memories* (RAM), electrical power provides the heat that is necessary for transformations between amorphous and crystalline states, which can be distinguished subsequently by their pronounced difference in electrical conductivity.[2–5]

To meet future requirements for multimedia applications of such phase change media, a higher data transfer rate is required. This can only be achieved by accelerating the time-limiting factor, which is the crystallization process in both optical and electronic media. Therefore, it is essential to understand crystallization kinetics of phase change alloys. For optical data storage, depending on the composition of the alloy, two mechanisms of recrystallization have been observed. For instance, AgIn-doped Sb_2Te (the material of choice in DVD-RW) recrystallizes by the growth of the crystalline phase from the rim of the amorphous mark.[6] In contrast, $Ge_4Sb_1Te_5$ and $Ge_2Sb_2Te_5$ (the latter is the material of choice in DVD-RAM) recrystallize by nucleation and subsequent growth of crystals inside the amorphous mark.[7] We recently showed[8] that nucleation rather than growth controls the recrystallization mechanism: All three alloys mentioned above have similar growth velocities around 150 °C, but the nucleation characteristics of the GeSbTe alloys differ remarkably from those of AgIn–Sb_2Te. It is plausible that these observations qualitatively hold for higher temperatures under operating conditions of phase change media. Hence, it is important to understand nucleation in Te alloys better. In this article, we analyze crystal nucleation and morphology by *ex situ* transmission electron microscopy (TEM) measurements in the three alloys mentioned above. Based on these findings, we deduce nucleation parameters for the GeSbTe alloys by further analyzing crystal size distribution measurements obtained in an earlier work by atomic force microscopy (AFM).[8]

II. EXPERIMENTAL TECHNIQUES

Thin films (30 and 350 nm) of compositions $Ge_4Sb_1Te_5$, $Ge_2Sb_2Te_5$, and $Ag_{0.055}In_{0.065}Sb_{0.59}Te_{0.29}$ (hereafter AgIn–Sb_2Te) were prepared by direct current magnetron sputtering on 640-μm-thick Si (100) wafers from a single target. The background pressure was approximately 10^{-6} mbar and the working pressure during sputtering in Ar ambient was 7×10^{-3} mbar. The sputtering power was 100 W. The deposition rate was approximately 0.5 nm/s and the target-substrate distance was 5 cm. As determined from x-ray-diffraction (XRD) and TEM measurements, the structure of the as-deposited films was entirely amorphous, i.e., no evidence of partial crystallization during deposition was found.

[a]Electronic mail: kalb@deas.harvard.edu; also at I. Physikalisches Institut der RWTH Aachen, 52056 Aachen, Germany.
[b]Electronic mail: spaepen@deas.harvard.edu

A. Observations of crystal morphology by *ex situ* TEM

The amorphous samples of the three alloys mentioned above were partially crystallized by annealing in a high-precision furnace of a Perkin Elmer Pyris 1 differential scanning calorimeter (DSC) in an argon atmosphere. The progress of crystallization was observed subsequently by a Digital Instruments 3100 AFM in TappingMode™ as described earlier.[8] Subsequently, self-supporting discs for TEM plan view measurements were prepared from the partially crystallized samples (film thickness: 30 nm) by ultrasonic disc cutting (Gatan Model 601), dimple grinding (Gatan Model 656), and ion milling (Gatan Model 691). For $Ge_4Sb_1Te_5$, additional cross-sectional TEM samples on copper washers were prepared from partially crystallized samples (film thickness: 350 nm) by mechanical tripod polishing and ion milling (Gatan Model 691). Such thick films were chosen to enable heterogeneous nucleation at the substrate and/or the film surface to be distinguished from homogeneous nucleation in the cross-sectional images.

A Philips TEM Model EM 420T operated at 100 kV was used to study the crystal morphology on the plan view samples in both bright field (BF) and centered dark field (CDF) modes. CDF was preferred towards displaced aperture dark field (DF) for better resolution. A JEOL 2010 FEG TEM/scanning transmission electron microscope (STEM) operated at 200 kV was used to study the cross-section samples in BF mode and to perform energy dispersive x-ray spectroscopy (EDS) on the plan view samples.

B. Measurements of nucleation parameters by *ex situ* AFM

$Ge_4Sb_1Te_5$ and $Ge_2Sb_2Te_5$ samples were alternately annealed in the furnace of the DSC and scanned in the AFM (between 2 and 9 cycle for each temperature) according to the method described earlier.[8] The time at which a crystal was nucleated was determined for each crystal in the observed area by measuring its diameter and using the time-independent crystal-growth velocity determined previously[8] for back calculation.[9] This procedure was repeated for several temperatures, 5 °C apart. For these experiments, films of thickness 30 nm were used.

III. RESULTS AND DISCUSSION

A. Observations of crystal morphology by *ex situ* TEM

Figures 1–3 show a crystal for each of the three alloys in both BF and CDF modes. Upon tilting the sample in *image mode* (both BF and CDF), the contrast moved *continuously* over the crystal. This was observed for all three alloys and is demonstrated for $Ge_4Sb_1Te_5$ in Fig. 1 for three tilting angles. Upon tilting the sample in *selected area electron-diffraction* (SAD) *mode*, the location of the diffraction spots did not change for any of the alloys. Therefore, in all three alloys each observed growth formation is a single crystal (not a polycrystal) that is curved *continuously* (bend contours[10]). Using a double tilt holder, it was demonstrated for all alloys

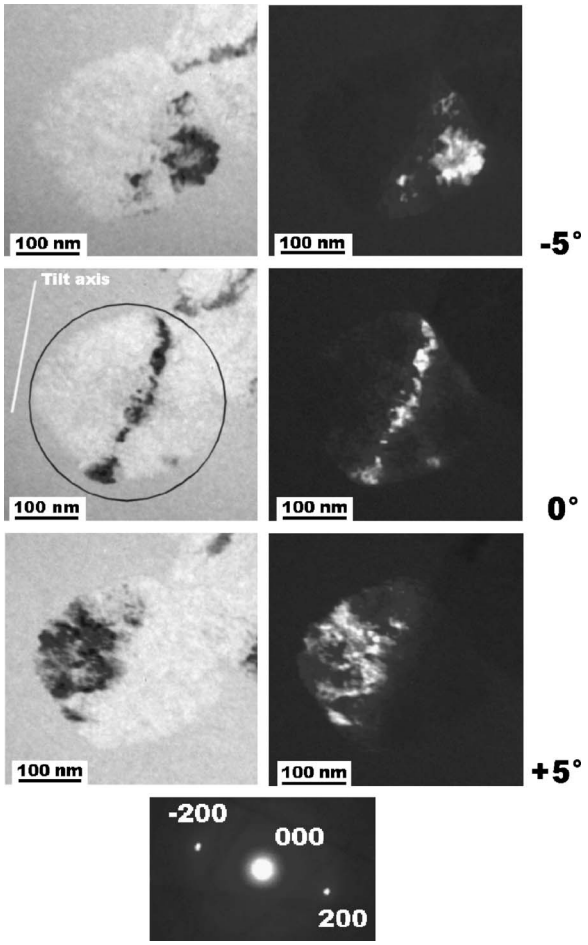

FIG. 1. Bright field (BF, left) and centered dark field (CDF, right) images of a $Ge_4Sb_1Te_5$ crystal for three tilting angles, 5° apart. The corresponding rotation-calibrated selected area diffraction (SAD) pattern is shown underneath. The location of the SAD aperture and the direction of the sample tilt axis are indicated in the BF image for 0°. The (200) diffraction was used for the CDF images. Before the TEM specimen preparation, the sample was annealed for 8.7 min at 160 °C.

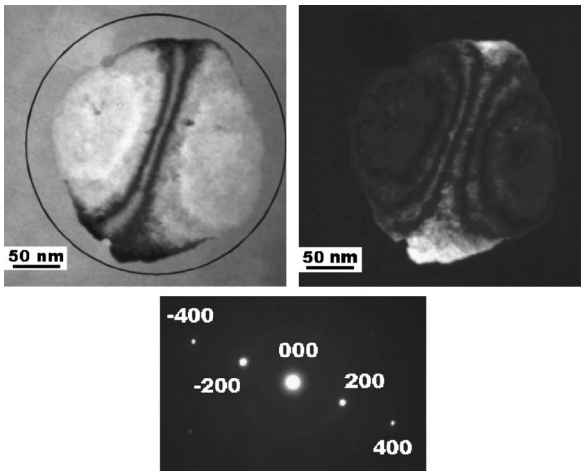

FIG. 2. Bright field (BF, left) and centered dark field (CDF, right) images of a $Ge_2Sb_2Te_5$ crystal. The corresponding rotation-calibrated SAD pattern is shown underneath. The location of the SAD aperture is indicated in the BF image. The (200) diffraction was used for the CDF image. Before the TEM specimen preparation, the sample was annealed for 600 min at 115 °C. The contrast change upon tilting is not indicated and is the same as in Fig. 1.

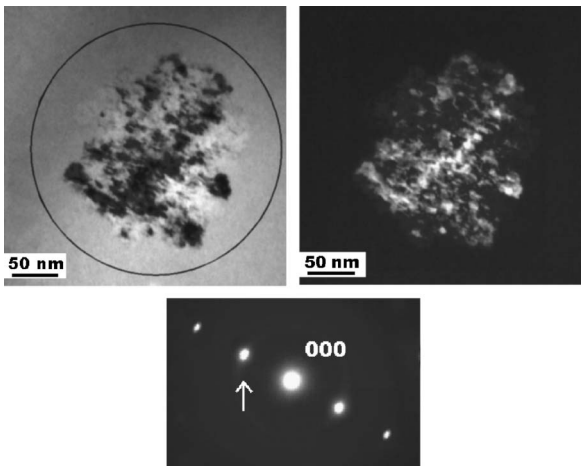

FIG. 3. Bright field (BF, left) and centered dark field (CDF, right) images of a AgIn–Sb_2Te crystal. The corresponding rotation-calibrated SAD pattern is shown underneath. The location of the SAD aperture is indicated in the BF image. The diffraction indicated by an arrow (Miller indices were not determined) was used for the CDF image. Before the TEM specimen preparation, the sample was annealed for 5.9 min at 160 °C. The contrast change upon tilting is not indicated and is the same as in Fig. 1.

and for each crystal that this curvature is present for any tilt axis in the film plane. Figure 1 shows only one example. Independent of its crystallographic orientation, each crystal, therefore, is shaped like a *spherical* cap. The bend contours are an intrinsic property of the crystal rather than a sample preparation artifact such as the bending of the entire foil. The radius of crystal curvature, as shown in Fig. 4, is on the order of 1 μm ($Ge_4Sb_1Te_5$ and AgIn–Sb_2Te) and 2 μm ($Ge_2Sb_2Te_5$), far smaller than the dimensions of the observable film. Hence, the observed magnitude of crystal curvature cannot continue in the amorphous surrounding. Crystal curvatures of similar magnitude as shown in Fig. 4 were reported by Kooi and co-workers[11,12] for $Ge_2Sb_2Te_5$ and $Sb_{3.6}Te$ and were ascribed to the volume change upon crystallization.[12] We carefully checked the sign of the curvature for many crystals on all three alloys and always found the same result (see Figs. 1 and 4). The same sign was also observed by Kooi and De Hosson.[12]

For AgIn–Sb_2Te, the amorphous-crystalline interface appears very rough, and the BF and CDF images exhibit a

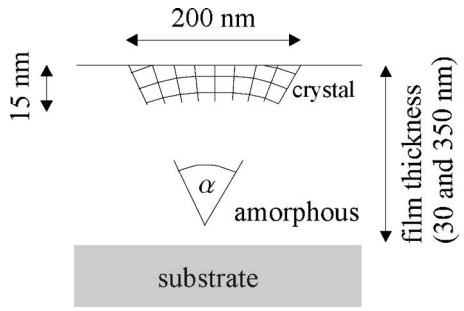

FIG. 4. Schematic illustration of heterogeneous crystal nucleation at the film surface. The crystals are only 15-nm thick normal to the film surface, but more than one order of magnitude wider in lateral direction. A typical tilt angle α for a 200-nm-wide crystal in a 30-nm-thick film is (11±2)° ($Ge_4Sb_1Te_5$ and AgIn–Sb_2Te), and (5±2)° ($Ge_2Sb_2Te_5$). The decrease in film height upon crystallization of 1–2 nm [Fig. 5(a)] is not shown here for simplicity. The sign of the curvature is the same for all alloys.

spotted diffraction contrast (features with size on the order of 10 nm). This is also true to a lesser extent for $Ge_4Sb_1Te_5$, but not for $Ge_2Sb_2Te_5$ (Figs. 1–3). In agreement with the discussion above (continuous crystal curvature) this contrast cannot be due to grains of size 10 nm having slightly different orientations because no arcs are visible in the SAD pattern (very short segments of the rings that are typically observed in polycrystalline films). The spotted diffraction contrast and the rough interface may be due to local strain fields caused by stacking faults,[10] which tilt the diffraction planes locally into and out of the Bragg condition. For AgIn–Sb_2Te, the stacking faults are probably due to the AgIn doping. Kooi *et al.*[11] observed this spotted diffraction contrast also for $Ge_2Sb_2Te_5$. This discrepancy with our observations may be the result of slight differences in stoichiometry and their effect on the formation of stacking faults. It should be noted that Kooi *et al.* use the terminology "colony of grains with a size 10 nm" rather than "spotted diffraction contrast" for this observation.[11] This terminology is not quite accurate, because the crystals are curved continuously. However, private communication with the authors revealed that their terminology was indeed used to describe the same "spotted diffraction contrast."

The BF image in Fig. 2 shows *two* parallel dark lines because the Bragg condition for the (200) planes is satisfied exactly in two locations due to the sample curvature.[10] The CDF image in Fig. 2 shows more bright lines because (a) double diffraction occurs, (b) diffraction occurs both at the front and at the back of the planes, and (c) CDF was used rather than DF for better image resolution. The pair of parallel dark lines in the BF image of Fig. 2 should also appear in the BF images for the other two alloys (Figs. 1 and 3) but cannot be separated because (a) the crystal curvature is larger for these alloys (Fig. 4) so that these lines move closer together in space,[10] and (b) the spotted diffraction contrast (as discussed above) prevents their resolution. Two parallel dark lines were also observed by Kooi and De Hosson[12] in BF images on $Sb_{3.6}Te$ crystals doped with 5% of Ge. Therefore, this fits well with the explanation given above: this alloy did not show spotted diffraction contrast so that these lines are revealed. Similarly, these lines were not observed by Kooi *et al.*[11] for $Ge_2Sb_2Te_5$ due to the spotted diffraction contrast in their images.

Analysis of the SAD patterns of many crystals showed that no obvious crystallographic texture was present in any of the alloys studied here. The SAD patterns match perfectly with a face-centered-cubic crystal structure for the GeSbTe alloys (lattice parameter: $a=6.02\pm0.04$ Å for $Ge_4Sb_1Te_5$ and $a=6.04\pm0.03$ Å for $Ge_2Sb_2Te_5$), in agreement with other studies of these alloys.[3,4,11,13] The camera length was calibrated using the SAD pattern of the Si substrate. Kooi *et al.*[11] observed texture in their TEM studies of $Ge_2Sb_2Te_5$: crystals with the {111} planes parallel to the surface were most abundant. The reason for this difference is unclear.

EDS line scans were performed across several crystals for all alloys. Within resolution (a few nanometers), no composition change upon crystallization could be observed, in agreement with the observation[8] that the crystal-growth velocity was time independent (interface controlled, not

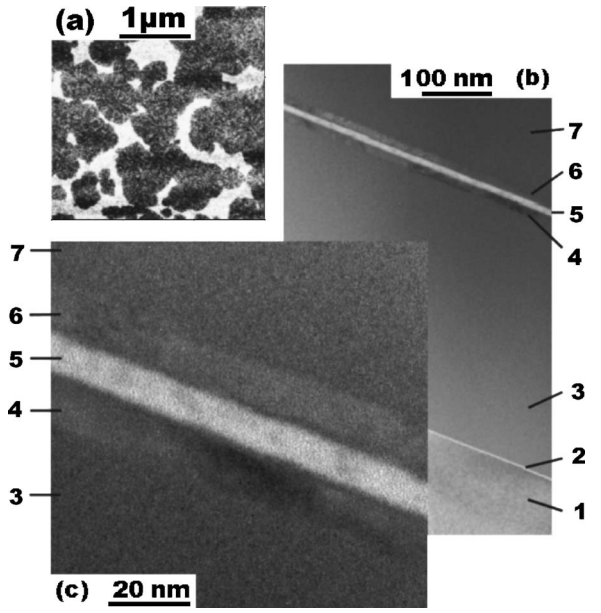

FIG. 5. $Ge_4Sb_1Te_5$ sample (film thickness: 350 nm) that was annealed for 36 min at 155 °C. (a) AFM image of the surface. Crystals (dark, height: −1 to −2 nm) are visible in the amorphous surrounding (bright, zero height). Note that the sample appears more than 70% crystallized. Crystals have a diameter of up to 500 nm. [(b) and (c)] Cross-sectional BF TEM micrographs of the sample shown in (a). Two samples are glued face to face. 1: Si substrate (sample 1); 2: natural SiO_2 layer (thickness 2 nm, sample 1); 3: amorphous $Ge_4Sb_1Te_5$ (sample 1); 4: crystalline $Ge_4Sb_1Te_5$ (sample 1); 5: glue; 6: crystalline $Ge_4Sb_1Te_5$ (sample 2); 7: amorphous $Ge_4Sb_1Te_5$ (sample 2). Normal to the film surface, the crystals are only about 15-nm thick. Comparison of (a) and (c) reveals that crystals are more than an order of magnitude wider than thick.

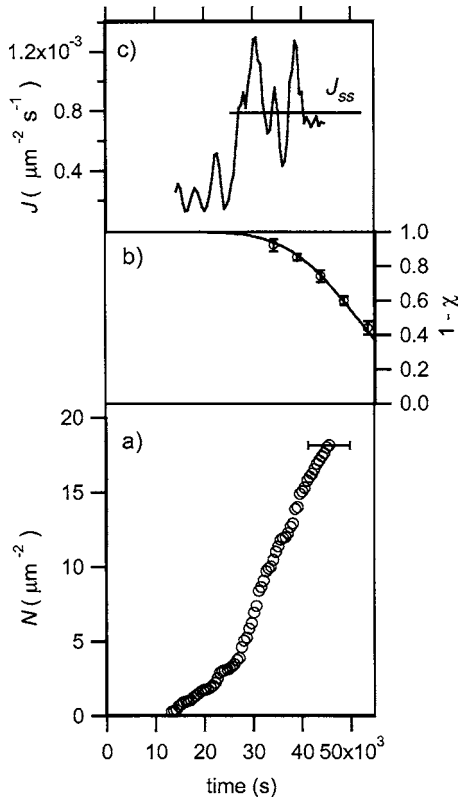

FIG. 6. Crystallization of $Ge_2Sb_2Te_5$ at 115 °C. (a) Number of crystals N obtained from diameter back calculation. The error bar on the last data point is the same for all other points and denotes the uncertainty in the time when a specific crystal is nucleated. No crystals nucleate for $t < 13\,000$ s (time lag τ). Transient effects dominate up to 25 000 s. For $t > 25\,000$ s, the steady state is reached. (b) Measured amorphous surface fraction $1-\chi$ after each anneal (data points), and interpolation (solid curve). (c) Calculated nucleation rate J according to Eq. (1). The steady-state nucleation rate J_{ss} is obtained by averaging the values for $t > 25\,000$ s (solid line).

diffusion-controlled growth[14]). The same was reported by Kooi and De Hosson[12] on their $Sb_{3.6}Te$ films.

Cross-sectional TEM on the alloy $Ge_4Sb_1Te_5$ (Fig. 5) showed that crystals only nucleate heterogeneously at the film surface. As also confirmed by SAD, heterogeneous nucleation at the Si substrate and homogeneous nucleation were not observed. The same was reported by Jeong *et al.*[15] for $Ge_2Sb_2Te_5$ films sputter deposited on Si substrates. Oxidation at the film surface may trigger nucleation for capillary reasons. Crystals are more than ten times wider than they are thick (Figs. 4 and 5). As the crystallographic orientations were observed to be random, this strong anisotropy cannot be the result of texture. It may be related to local strain effects (due to the density change upon crystallization[3,5,16]) that favor growth in the lateral direction and inhibit growth in the normal direction.

Kooi and De Hosson argue[12] that the large density change upon crystallization,[3,5,16] which induces a local change in film height,[17] is responsible for the appearance of bend contours for crystals that nucleate heterogeneously at the film surface. Their explanation probably applies to our alloys as well.

B. Measurements of nucleation parameters by *ex situ* AFM

Figure 6(a) shows the result of the back calculation of the time at which $Ge_2Sb_2Te_5$ crystals nucleated at 115 °C. The analysis is based on the observations of Sec. III A in two respects: First, the number of crystals is normalized per unit area rather than per unit volume because crystals only nucleate heterogeneously at the film surface (Fig. 5). Second, each growth formation is a bent *single* crystal (not a polycrystal), which justifies the back calculation of their nucleation time. For small times, no crystals nucleate, in agreement with *in situ* TEM observations by Ruitenberg *et al.*[18] and Privitera *et al.*[19] on $Ge_2Sb_2Te_5$ in the same temperature range. The time lag τ (Fig. 7) is defined as the time at which the first crystal (the one with the largest diameter) nucleates, counted from the beginning of the first isothermal anneal. For $AgIn-Sb_2Te$, the nucleation sites are exhausted at an early stage of the transformation.[8] The approximate time $\tilde{\tau}$ when the last crystal (the one with the smallest diameter) nucleates is therefore also indicated in Fig. 7 for this alloy. According to Table I, the activation energy for $\tilde{\tau}$ is larger than for τ for this alloy, so that the crystal diameter distribution becomes "sharper" with increasing temperature. The appearance of a nonzero time lag for $AgIn-Sb_2Te$ implies that the crystals in Figs. 1(a) and 1(b) of Ref. 8, which all have about the same diameter, were *not* grown from crystalline clusters that were already present *before* the anneal but were nucleated *during* the isothermal anneal. The time lag for $Ge_4Sb_1Te_5$ was zero within the uncertainty of measurement and is therefore not indicated in Fig. 7. A time lag on the order of 100 ns was

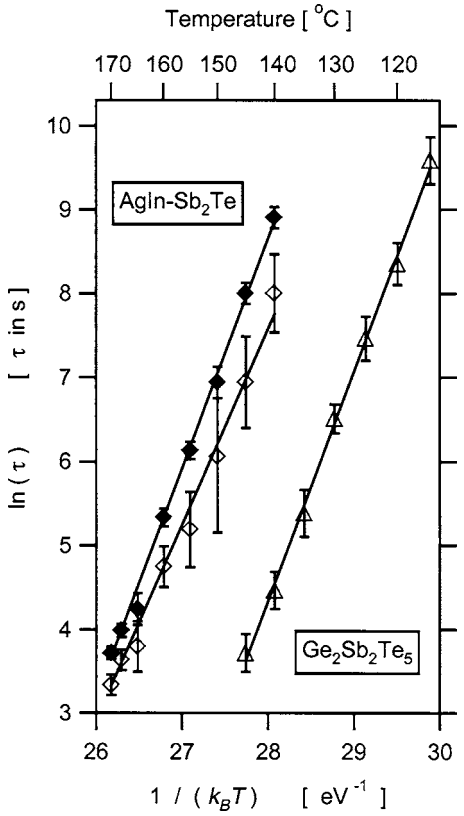

FIG. 7. Time lag for nucleation τ for AgIn–Sb_2Te (open squares) and $Ge_2Sb_2Te_5$ (open triangles). For the AgIn–Sb_2Te alloy, in which nucleation sites are exhausted in the early stage of the transformation (Ref. 8), the approximate time $\tilde{\tau}$ when the *last* crystal nucleates is also indicated (full squares). For $Ge_2Sb_2Te_5$, crystals nucleate throughout the entire transformation so that a statement on $\tilde{\tau}$ is not applicable. $Ge_4Sb_1Te_5$ is not included because the time lag was zero within the uncertainty of measurement. Fit parameters are listed in Table I.

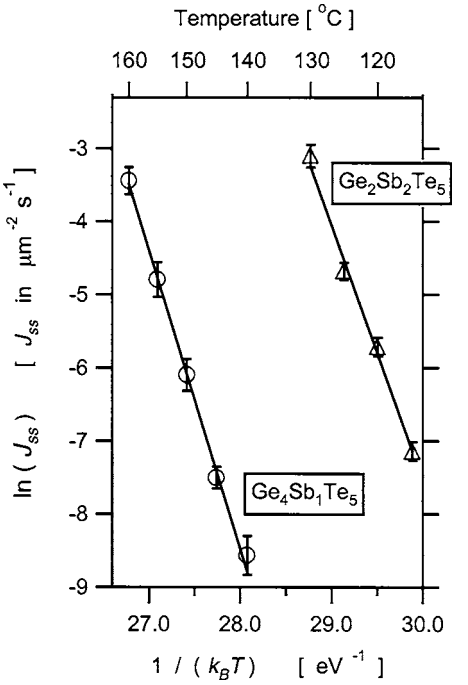

FIG. 8. Steady-state nucleation rate J_{ss} for $Ge_4Sb_1Te_5$ (circles) and $Ge_2Sb_2Te_5$ (triangles) as a function of temperature. AgIn–Sb_2Te is not included because the steady state is not reached as nucleation sites are exhausted at an early stage of the transformation (Ref. 8). Fit parameters are listed in Table II.

observed[20–23] by laser irradiation experiments for all three alloys at temperatures significantly above 200 °C (statements on the exact temperature in the laser experiments are complicated). Therefore, it is expected that the time lag for $Ge_4Sb_1Te_5$ is greater than zero also for temperatures below 200 °C but too small to be revealed in our experiments due to insufficient time resolution.

The nucleation rate $J(t_i)$ at time t_i was obtained from

$$J(t_i) = \frac{\dot{N}(t_i)}{1-\chi(t_i)}, \tag{1}$$

where $N(t_i)$ is the crystal number in Fig. 6(a). The time derivative $\dot{N}(t_i)$ at time t_i is obtained from the slope of a linear fit to five data points of N in the range $[t_{i-2}, t_{i+2}]$ in Fig. 6(a). $\chi(t_i)$ is the crystallized surface fraction at time t_i, which was obtained by interpolating the measured crystallized fractions after each anneal[24] [Fig. 6(b)]. The factor $1/1-\chi(t_i)$ normalizes $\dot{N}(t_i)$ because crystals can only nucleate in the untransformed fraction $1-\chi(t_i)$ of the surface. $J(t_i)$ is plotted in Fig. 6(c). Although the differentiated data is noisy, it can clearly be seen that the nucleation rate is lower for $t<25\,000$ s than for $t>25\,000$ s. Transient effects appear predominant for $t<25\,000$ s, whereas the steady state is reached for $t>25\,000$ s. The steady-state nucleation rate J_{ss} is determined as the average of the data for $t>25\,000$ s [Fig. 6(c)]. This procedure was repeated for all temperatures. J_{ss} is plotted as a function of temperature in Fig. 8 for the GeSbTe alloys. AgIn–Sb_2Te is not included in this plot because the steady state is not reached due to exhaustion of nucleation sites.[8] The fit parameters for the Arrhenius fits in Fig. 8 are listed in Table II.

According to the classical theory of steady-state nucleation,[14] the work to form a critical nucleus, W_c, can be found from

TABLE I. Fit parameters for the time lag for nucleation τ [Arrhenius fit: $\ln(\tau)=\ln(\tau_0)+E_\tau/(k_BT)$] and the approximate time $\tilde{\tau}$ when the last crystal nucleated [Arrhenius fit: $\ln(\tilde{\tau})=\ln(\tilde{\tau}_0)+E_{\tilde{\tau}}/(k_BT)$] in Fig. 7.

Alloy	$\ln(\tau_0)$ (τ_0 in s)	E_τ (eV)	$\ln(\tilde{\tau}_0)$ ($\tilde{\tau}_0$ in s)	$E_{\tilde{\tau}}$ (eV)
$Ge_2Sb_2Te_5$	−72.36±3.77	2.74±0.13	n/a	n/a
AgIn–Sb_2Te	−57.75±4.86	2.33±0.18	−67.99±1.56	2.74±0.06

TABLE II. Fit parameters for the steady-state nucleation rate J_{ss} [Arrhenius fit: $\ln(J_{ss})=\ln(J_0)-E_J/(k_BT)$] in Fig. 8. The activation energy for growth is given for comparison. The work to form the critical nucleus W_c is obtained from Eq. 2.

Alloy	$\ln(J_0)$ (J_0 in $\mu m^{-2}\,s^{-1}$)	E_J (eV)	E_u[a] (eV)	W_c (eV)
$Ge_4Sb_1Te_5$	105.96±5.53	4.09±0.20	2.74±0.03	1.35±0.23
$Ge_2Sb_2Te_5$	97.53±4.86	3.50±0.17	2.35±0.05	1.15±0.22

[a]From Ref. 8.

$$W_c = E_J - E_u, \tag{2}$$

where E_u is the activation energy for the growth velocity taken from Ref. 8 and E_J the activation energy for the steady-state nucleation rate (Table II). W_c is given in Table II. As the nucleation is heterogeneous (Fig. 5 and Ref. 15), Eq. (2) provides a lower limit for the critical work for homogeneous nucleation.

Using the same analysis, Privitera *et al.*[19] found an activation energy for the steady-state nucleation rate of (2.9 ± 0.5) eV for $Ge_2Sb_2Te_5$ by *in situ* TEM, which is lower than our value of (3.50 ± 0.17) eV (Table II). As a result, they obtain a value for W_c of less than 1 eV, which is lower than ours. The deviation is most likely the result of differences in surface and interface energies in the two experiments.

IV. CONCLUSIONS

(1) Earlier observations by Kooi and co-workers[11,12] on similar Te alloys were confirmed: only heterogeneous nucleation of bent single crystals occurs.
(2) The crystals are much wider than thick. Their thickness is much less than the film thickness for 350-nm-thick films so that most of the film remains amorphous during the crystallization of the surface.
(3) Analysis of the crystal size distribution at temperatures around 150 °C revealed a thermally activated time lag for nucleation τ and an early exhaustion of nucleation sites for $AgIn-Sb_2Te$, but continuous transient nucleation for the GeSbTe alloys. The time lag was thermally activated for $Ge_2Sb_2Te_5$, while it was zero within the uncertainty of measurement for $Ge_4Sb_1Te_5$. A higher time resolution may reveal the time lag for this alloy. The steady-state nucleation rate J is thermally activated for the GeSbTe alloys.
(4) The nucleation parameters determined in this work are useful for modeling crystallization kinetics.

ACKNOWLEDGMENTS

One of the authors (J.K.) acknowledges the Deutscher Akademischer Austauschdienst and the Studienstiftung des Deutschen Volkes for financial support. Another author (F.S.) acknowledges partial support from the Alexander-von-Humboldt-Stiftung. W. J. MoberlyChan and B. J. Kooi are acknowledged for helpful discussions on the TEM observations. Work at Harvard is supported in part by the MRSEC program of the NSF.

[1] N. Yamada, MRS Bull. **21**, 48 (1996).
[2] S. Hudgens and B. Johnson, MRS Bull. **29**, 829 (2004).
[3] D. Wamwangi, W. K. Njoroge, and M. Wuttig, Thin Solid Films **408**, 310 (2002).
[4] I. Friedrich, V. Weidenhof, W. Njoroge, P. Franz, and M. Wuttig, J. Appl. Phys. **87**, 4130 (2000).
[5] W. K. Njoroge and M. Wuttig, J. Appl. Phys. **90**, 3816 (2001).
[6] H. J. Borg, M. van Schijndel, J. C. N. Rijpers, H. H. R. Lankhorst, G. Zhou, M. J. Dekker, I. P. D. Ubbens, and M. Kuijper, Jpn. J. Appl. Phys., Part 1 **40**, 1592 (2001).
[7] J. H. Coombs, A. P. J. M. Jongenelis, W. van Es-Spiekman, and B. A. J. Jacobs, J. Appl. Phys. **78**, 4918 (1995).
[8] J. Kalb, F. Spaepen, and M. Wuttig, Appl. Phys. Lett. **84**, 5240 (2004).
[9] U. Köster and A. Blanke, Scr. Metall. **17**, 495 (1983).
[10] D. B. Williams and C. B. Carter, *Transmission Electron Microscopy* (Plenum, New York, 1996).
[11] B. J. Kooi, W. M. G. Groot, and J. Th. M. De Hosson, J. Appl. Phys. **95**, 924 (2004).
[12] B. J. Kooi and J. Th. M. De Hosson, J. Appl. Phys. **95**, 4714 (2004).
[13] N. Yamada and T. Matsanuga, J. Appl. Phys. **88**, 7020 (2000).
[14] J. W. Christian, *The Theory of Transformations in Metals and Alloys* 2nd ed. (Pergamon, North-Holland, Amsterdam, 1975).
[15] T. H. Jeong, M. R. Kim, H. Seo, S. J. Kim, and S. Y. Kim, J. Appl. Phys. **86**, 774 (1999).
[16] V. Weidenhof, I. Friedrich, S. Ziegler, and M. Wuttig, J. Appl. Phys. **86**, 5879 (1999).
[17] T. P. Leervad Pedersen, J. Kalb, W. K. Njoroge, D. Wamwangi, M. Wuttig, and F. Spaepen, Appl. Phys. Lett. **79**, 3597 (2001).
[18] G. Ruitenberg, A. K. Petford-Long, and R. C. Doole, J. Appl. Phys. **92**, 3116 (2002).
[19] S. Privitera, C. Bongiorno, E. Rimini, and R. Zonca, Appl. Phys. Lett. **84**, 4448 (2004).
[20] V. Weidenhof, I. Friedrich, S. Ziegler, and M. Wuttig, J. Appl. Phys. **89**, 3168 (2001).
[21] I. Friedrich, V. Weidenhof, S. Lenk, and M. Wuttig, Thin Solid Films **389**, 239 (2001).
[22] H.-W. Wöltgens, R. Detemple, I. Friedrich, W. K. Njoroge, I. Thomas, V. Weidenhof, S. Ziegler, and M. Wuttig, Mater. Res. Soc. Symp. Proc. **674**, V1.3 (2001).
[23] S. Ziegler, Ph.D. thesis, Rheinisch-Westfälische Technische Hochschule, 2005.
[24] The data for χ in Fig. 6(b) were measured by successive anneals of the same sample. The same values were obtained for single anneals of the same overall length.